Pharm Res (2012) 29:1960–1976
DOI 10.1007/s11095-012-0724-6

RESEARCH PAPER

# Drug–Drug Interaction Potential of Marketed Oncology Drugs: *In Vitro* Assessment of Time-Dependent Cytochrome P450 Inhibition, Reactive Metabolite Formation and Drug–Drug Interaction Prediction

Jane R. Kenny • Sophie Mukadam • Chenghong Zhang • Suzanne Tay • Carol Collins • Aleksandra Galetin • S. Cyrus Khojasteh

Received: 9 December 2011 / Accepted: 27 February 2012 / Published online: 14 March 2012


## ABSTRACT

***Purpose*** To evaluate 26 marketed oncology drugs for time-dependent inhibition (TDI) of cytochrome P450 (CYP) enzymes. Evaluate TDI-positive drugs for potential to generate reactive intermediates. Assess clinical drug–drug interaction (DDI) risk using static mechanistic models.

***Methods*** Human liver microsomes and CYP-specific probes were used to assess TDI in a dilution shift assay followed by generation of $K_I$ and $k_{inact}$. Reactive metabolite trapping studies were performed with stable label probes. Static mechanistic model was used to predict DDI risk using a 1.25-fold AUC increase as a cut-off for positive DDI.

***Results*** Negative TDI across CYPs was observed for 13/26 drugs; the rest were time-dependent inhibitors of, predominantly, CYP3A. The $k_{inact}/K_I$ ratios for 11 kinase inhibitors ranged from 0.7 to 42.2 ml/min/$\mu$mol. Stable label trapping agent–drug conjugates were observed for ten kinase inhibitors. DDI predictions gave no false negatives, one true negative, four false positives and three true positives. The magnitude of DDI was overestimated irrespective of the inhibitor concentration selected.

***Conclusions*** 13/26 oncology drugs investigated showed TDI potential towards CYP3A, formation of reactive metabolites was also observed. An industry standard static mechanistic model gave no false negative predictions but did not capture the modest clinical DDI potential of kinase inhibitors.

**KEY WORDS** drug-drug interaction · kinase inhibitors · prediction · reactive metabolites · time-dependent CYP inhibition

## ABBREVIATIONS

| | |
|---|---|
| AUC | area under the curve |
| $C_{av}$ | average plasma concentration |
| $C_{max}$ | maximum plasma concentration |
| CYP | cytochrome P450 |
| DDI | drug–drug interaction |
| HLM | human liver microsomes |
| LC | liquid chromatography |
| MS/MS | tandem mass spectrometry |
| NME | new molecular entity |
| PBPK | physiologically based pharmacokinetic modeling |
| TDI | time-dependent inhibition |

## INTRODUCTION

Drug interactions in the field of oncology are commonplace and may lead to serious adverse events in the clinic (1). The current treatment for oncology is divided into two broad classes: cytotoxic chemotherapeutic agents whose efficacy is

This work was presented in part at the PSWAAPS meeting, 2010, New Orleans.

**Electronic supplementary material** The online version of this article (doi:10.1007/s11095-012-0724-6) contains supplementary material, which is available to authorized users.

J. R. Kenny (✉) • S. Mukadam • C. Zhang • S. Tay • S. C. Khojasteh
Department of Drug Metabolism and Pharmacokinetics
Genentech Inc.
1 DNA Way, MS412A, South San Francisco, California 94080, USA
e-mail: kenny.jane@gene.com

C. Collins
Department of Pharmaceutics, University of Washington
Seattle, USA

A. Galetin
Center for Applied Pharmacokinetic Research
School of Pharmacy and Pharmaceutical Sciences
The University of Manchester
Manchester, UK

limited by their toxicity, and targeted therapies/protein kinase inhibitors (2). Generally, cytotoxic chemotherapeutic agents are administered at doses close to the maximum that can be tolerated (3), and historically, for these agents drug–drug interactions (DDIs) have been largely ignored (4). Conversely, targeted therapies or kinase inhibitors are better tolerated and are potentially administered for long periods of time (until disease progression) and in most cases, continuously (5). Nevertheless many of these therapies are considered narrow therapeutic index drugs. These drugs exhibit extensive inter-individual variability in their pharmacokinetics (3), and greater than 90 % of cancer patients are treated with more than two different drugs concurrently. These factors present a DDI risk to patients, and the role of oncology therapies as either victim or perpetrator of DDI needs to be carefully evaluated and balanced with relative risk:benefit ratios for patients. As such, it is apparent that DDIs need to be more widely considered in the oncology field (4,6,7).

Pharmacokinetic DDI may result in elevated exposure which may exacerbate the adverse events, such as skin toxicities, nausea and hematological effects, associated with kinase inhibitors (8). Reports of cytochrome P450 (CYP)-mediated DDI for kinase inhibitors have predominantly focused on the inhibitors' role as victim drugs (9–12). Clinical reports on the kinase inhibitors as perpetrators of DDI suggest that the magnitude of inhibition is modest, typically resulting in a less than 2-fold change in exposure of the victim drug (13). However, dasatinib, erlotinib, gefitinib and lapatinib have been shown to cause modest time-dependent inhibition (TDI) *in vitro* (14–17), and the translation of this *in vitro* TDI into a clinically significant DDI risk is still being assessed. For new therapies still in the discovery or development phases, an evaluation of the *in vitro* TDI liabilities for current marketed drugs is a valuable aid when considering the risk:benefit profile of a new molecular entity (NME).

The industry standard is to screen for CYP inhibition, including TDI, early in the drug discovery process. This is a regulatory requirement as a compound progresses to the clinic. With increased understanding of the complexity of TDI and advances in *in vitro* methodologies, it is now possible to identify compounds with even weak interaction potential (18). The time- and concentration-dependent nature of this inhibition, alongside its irreversible nature, make assessment of DDI risk important. Various models exist to evaluate DDI potential, ranging from mechanistic static to physiologically based pharmacokinetic (PBPK) models (such as implemented in the Simcyp simulator® software). These models have been demonstrated to accurately predict the magnitude of DDI due to TDI when the right input parameters are given (19–23). However, these models can in some instances result in overprediction of DDI magnitude depending on the initial model assumptions, parameter estimates used and model complexity (20,24). PBPK models, although capable of simulating changing drug concentration in a dynamic way, require rich input data for the most accurate simulations. These data are often not available for compounds early in drug discovery and this, in addition to recommendations from regulatory authorities (www.fda.gov//downloads/Drugs/DevelopmentApprovalProcess/DevelopmentResources/DrugInteractionsLabeling/UCM269209.pdf), make the mechanistic static models attractive when either focusing on TDI in isolation (19,20,25) or expanded to account for multiple interaction mechanisms (26).

The aim of the work presented here was to comprehensively evaluate the *in vitro* time-dependent CYP inhibition of 26 marketed oncology drugs, 12 of which were kinase inhibitors, (Fig. 1) using standard CYP probe substrates. Additionally, we assessed formation of reactive metabolites of these kinase inhibitors *in vitro* using common trapping agents. Finally, we attempted to extrapolate *in vitro* inhibition to eight reported clinical DDI studies with midazolam, simvastatin, everolimus and atorvastatin using a mechanistic static model accounting for both TDI and reversible inhibition (where applicable). The impact of inhibitor and enzyme related parameters in the mechanistic static model on the prediction accuracy of DDIs was investigated. In particular, different surrogates for inhibitor concentration, variability in plasma protein binding and CYP3A4 turnover rate constants in liver relative to intestine. Implications of the findings and ability of the mechanistic static model to assess DDI potential of kinase inhibitors are discussed.

## MATERIALS AND METHODS

### Materials

1′-Hydroxymidazolam was purchased from Cerilliant (Round Rock, TX). 1′-Hydroxymidazolam-d3 was purchased from High Standard Products (Westminster, CA). 1′-Hydroxymidazolam-$^{13}$C3, mifepristone and (*S*)-warfarin were purchased from US Biological (Swampscott, MA). 3,4-Methylenedioxymethamphetamine, 7,8-benzoflavone, dextromethorphan, dimethylsulfoxide (DMSO), everolimus, furafylline, glutathione, hydrobromide, ketoconazole, methotrexate, methoxylamine, phenacetin, phenyl-d5-7-hydroxywarfarin, potassium cyanide, propranolol, quinidine, sulfaphenazole, temozolomide, ticlopidine, troleandomycin and testosterone were purchased from Sigma Aldrich (St. Louis, MO). 5′-Flurouracil, cisplatin and docetaxel were purchased from LKT Laboratories (St. Paul, MN). (±)-4′-Hydroxymephenytoin-d3, 6-β-hydroxytestosterone-d3, acetaminophen-d4, dextrorphan-d3, capecitabine,

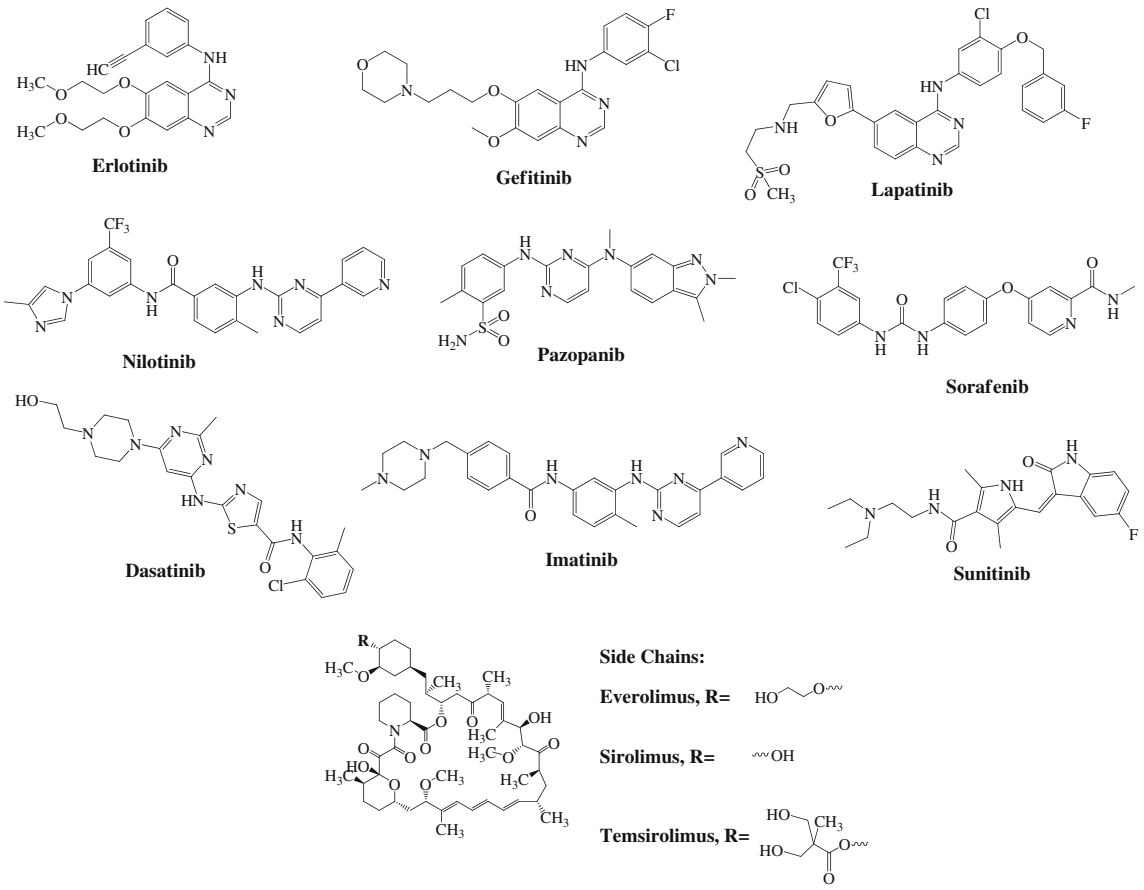


**Fig. 1** Chemical structures of the kinase inhibitors.

dasatinib, doxorubicin, gestodene, paclitaxel, pemetrexed, (*S*)-(+)-*N*-3-benylnirvanol, sunitinib and vorinostat were purchased from Toronto Research Chemicals (North York, ON, Canada). Cyclophosphamide was purchased from Acros Organics (Geel, Belgium). Erlotinib, gefitinib, imatinib, irinotecan, lapatinib, pazopanib, sirolimus (rapamycin), sorafenib and sunitinib were purchased from LC Laboratories (Woburn, MA). Etoposide was purchased from Tocris Bioscience (Ellisville, MO). Midazolam was purchased from Spectrum Chemicals (Gardena, CA). β-Nicotinamide adenine dinucleotide phosphate, (reduced form; NADPH) was purchased from Calbiochem (San Diego, CA) or Sigma Aldrich (St. Louis, MO). Nilotinib and temsirolimus were purchased from LC Laboratories (Woburn, MA) or VWR International (West Chester, PA). (*S*)-Mephenytoin was purchased from Enzo Life Sciences International (Plymouth Meeting, PA). Stable labeled glutathione ($^{13}C$, $^{15}N$ on glycine) and methoxylamine-d3 were purchased from Cambridge Isotope Laboratories, Inc. (Andover, MA). Stable labeled potassium cyanide -$^{13}C$-$^{15}N$ was purchased from Isotec Inc (Des Plaines, IL). Topotecan was purchased from Tecoland Corp (Edison, NJ). Vorinostat was purchased from Selleck Chemicals LLC (Houston, TX). All chemicals were of the highest qualities available and provided in solid form (with the exception of 1′-hydroxymidazolam, which was provided as 100 μg/ml stock in methanol and stored at−20 °C). HPLC grade acetonitrile, formic acid, glacial acetic acid and water were purchased from VWR International (West Chester, PA).

Pooled male and female human liver microsomes (HLMs) were purchased from BD Biosciences (50 donor pool, 86 % Caucasian; CYP3A4 86 pmol/mg and CYP3A5 13 pmol/mg by Western blot; San Jose, CA) and CellzDirect (20 donor pool; 86 % Caucasian, Durham, NC). Male human plasma (treated with potassium EDTA) was purchased from Bioreclamation LLC (Westbury, NY). Potassium phosphate buffer (100 mM; pH 7.4) and phosphate buffered saline (PBS, pH 7.4) were prepared by the Media Preparation Facility at Genentech, Inc.

## Assessment of TDI Liability of Five Major CYP Isoforms

TDI of CYP1A2, CYP2C9, CYP2C19, CYP2D6 and CYP3A were evaluated using an automated AUC shift dilution assay adapted from methodology described by

Obach *et al.* (2007)(20). In brief, the test compound in DMSO (0, 1, 10, 50 and 100 μM) was incubated with pooled HLMs (0.3 mg/ml) in potassium phosphate buffer (100 mM; pH 7.4) in the presence and absence of NADPH (1 mM) for 30 min at 37 °C. The final solvent concentration was 1 % DMSO (*v*/*v*), and the incubation volume was 150 μl. After this initial incubation, a 10-fold dilution was performed into six separate secondary incubations containing NADPH (1 mM) and a CYP probe in potassium phosphate buffer (100 mM; pH 7.4); the secondary incubations were allowed to proceed for 10–40 min depending on the enzyme being assessed. The probe substrates, probe concentrations and incubation times for the five CYPs were as reported for reversible CYP inhibition (27) and were as follows: CYP1A2, phenacetin (100 μM; 30 min); CYP2C9, *S*-warfarin (4 μM; 30 min); CYP2C19, (*S*)-mephenytoin (120 μM; 40 min); CYP2D6, dextromethorphan (10 μM; 10 min); CYP3A, testosterone (100 μM; 10 min) and midazolam (4 μM; 10 min). Under these conditions, the formation rate of CYP-specific metabolites was within the linear range. The final solvent concentration in the secondary incubation was 0.1 % *v*/*v* and the incubation volume was 70 μl. The secondary incubations were quenched with addition of formic acid (6 %) in acetonitrile (35 μl) containing the deuterated metabolite internal standard specific for each CYP probe. Following quenching, the samples were pooled for analysis by LC-MS/MS as described below. The assay was conducted using a 384-well plate format and fully automated protocol on a BioCel 1200 from Agilent Technologies (Santa Clara, CA).

Aliquots (25 μl) were analyzed by LC-MS/MS for CYP-specific metabolites of probe substrates. The equipment consisted of an Agilent 1200 series HPLC system (Palo Alto, CA), an HTS PAL autosampler from CTC Analytics (Carrboro, NC) equipped with a Cohesive LX-2 Multiplexing system from Thermo Scientific (Franklin, MA) coupled to a Triple Quad 5500™ mass spectrometer, equipped with an electrospray ionization (ESI) source from AB Sciex (Foster City, CA). The mass spectrometer was operated under multiple reaction monitoring (MRM) conditions in positive/negative switching mode. A Hypersil Gold column (1.9 micron, 50×2.1 mm) from Thermo Scientific and mobile phases containing 0.01 % formic acid in water (A) and 0.01 % formic acid in acetonitrile (B) were used for chromatographic separation. The stepwise linear gradient was 1 % B (0–0.4 min), 10–40 % B (0.42–2.7 min), 40–95 % B (2.7–2.95 min), and 1 % B (2.96–4.4 min). The total run time was 4.4 min using a flow rate of 0.55 ml/min.

The CYP-specific metabolites of probe substrates were quantified by LC-MS/MS using the ratio of metabolite peak area to that of the internal standard. The amount of metabolite formed at each concentration relative to the vehicle control (or percent remaining activity) was calculated and plotted against inhibitor concentration. The areas under the curve (AUCs) were calculated and $IC_{50}$ values were estimated by nonlinear regression using XLfit 4.0 from IDBS (Guildford, Surrey, UK). The difference between the AUCs in the presence and absence of NADPH in the pre-incubation was compared, and an AUC shift (%) was determined as described in Eq. 1 so that increasing TDI resulted in increasing AUC shift values between 0 and 100. Any compounds with a greater than nominal 15 % shift in AUC were flagged as exhibiting potential TDI.

$$\text{AUC Shift (\%)} = \left(1 - \frac{\text{AUC with NADPH pre-incubation}}{\text{AUC without NADPH pre-incubation}}\right) \times 100 \quad (1)$$

## Determination of CYP3A $K_I$ & $K_{inact}$

The inhibitor concentration that supports half the maximal rate of inactivation ($K_I$) and the maximal rate of enzyme inactivation ($k_{inact}$) for CYP3A were determined manually in HLMs. The test compound (0, 0.1, 0.62 1.9 5.6, 16.7, 50, and 100 μM) was incubated at 37 °C with pooled HLMs (0.6 mg/ml) and NADPH (1.3 mM) in potassium phosphate buffer (100 mM; pH 7.4) for 0.5, 2.5, 9, 16, and 25 min with midazolam as a probe substrate and for 0.5, 3, 8, 17 and 30 min with testosterone as a probe substrate. The final incubation volume was 100 μl. The final solvent content in the incubation was 0.05 % DMSO and 0.95 % acetonitrile. After this initial incubation, a 20-fold dilution was performed into a secondary incubation containing midazolam (16 μM) or testosterone (250 μM) and NADPH (1.3 mM) in potassium phosphate buffer (100 mM; pH 7.4). The secondary incubation (200 μl final volume) was allowed to proceed at 37 °C for 4 (midazolam) or 10 min (testosterone) before the reaction was quenched with formic acid (3 %) in acetonitrile (50 μl) containing internal standard (1′-hydroxymidazolam-d3 [0.1 μM] or 6-β-hydroxytestosterone-d3 [1 μM]). The samples were then centrifuged (2000 × g for 5 min) and analyzed by LC-MS/MS as described below.

Aliquots (10 μl) were analyzed by LC-MS/MS for either 1′-hydroxymidazolam or 6-β-hydroxytestosterone. The equipment consisted of an Agilent 1200 series HPLC system, an HTS PAL autosampler from CTC Analytics equipped with a Cohesive LX-2 Multiplexing system from Thermo Scientific coupled to an API4000™ mass spectrometer, equipped with an ESI source from AB Sciex. The mass spectrometer was operated under MRM conditions in the positive ion mode. A C-18 Hypersil Gold column (1.9 μm, 50×2.1 mm) from Thermo Scientific and mobile phases of 0.1 % formic acid in water (A) and 0.1 % formic acid in acetonitrile (B) were used for chromatographic separation. For midazolam, the stepwise linear gradient was 5 % B (0–0.1 min), 30 % B (0.1–1.2 min), and 95 % B (1.2–1.9 min).

The total run time was 3 min using a flow rate of 0.4 ml/min. For testosterone, the stepwise linear gradient was 5 % B (0–0.1 min), 30 % B (0.1–1.2 min), 95 % B (1.2–1.9 min), and 5 % B (1.91–4.0 min). The total run time was 4 min using a flow rate of 0.4 ml/min.

CYP-specific metabolites of probe substrates were quantified by LC-MS/MS using the ratio of metabolite peak area to that of the internal standard. The amount of metabolite formed at each concentration relative to a vehicle control (or percent remaining activity) was calculated, and $k_{obs}$ (observed first-order inactivation rate constant) was determined by linear fit of the natural logarithm of percent remaining activity *versus* time for each concentration of test compound ([I]). Apparent $K_I$ and $k_{inact}$ were estimated using nonlinear regression in Prism 5 from GraphPad Software Inc. (La Jolla, USA) using the following equation:

$$k_{obs} = \frac{[I] \cdot k_{inact}}{[I] + K_I} \quad (2)$$

## Assessment of Reactive Metabolite Formation

The formation of reactive metabolites was evaluated in HLMs using stable labeled trapping agents (glutathione, potassium cyanide and methoxylamine) to aid detection. The use of the stable labels for trapping studies allows for enhanced selectivity of mass spectrometry detection, and the concentration of trapping agents was staged to minimize CYP inhibition (23,28,29).

Briefly, the test compound (20 μM) was incubated (37 °C; 60 min) with pooled HLMs (1 mg/ml), NADPH (1 mM) and a 1:1 ratio of unlabeled and labeled trapping agent, namely, glutathione (1 mM), methoxylamine (0.5 mM) or potassium cyanide (1 mM) in potassium phosphate buffer (100 mM, pH 7.4). The final incubation volume was 200 μl with a solvent concentration of 0.02 % DMSO and 0.38 % acetonitrile for glutathione and methoxylamine and 0.38 % methanol for potassium cyanide. The reaction was quenched by addition of acetone (500 μl), samples were centrifuged (2000×g for 10 min), the supernatant removed and evaporated to dryness using an Evaporex EVX-192 from Apricot Designs (Monrovia, CA). Sample was reconstituted in methanol:water (1:1 *v/v*; 200 μl) for analysis by LC-MS/MS.

Aliquots (17 μl) were analyzed for conjugate formation using accurate mass and isotope pattern filtering software MsXelerator from MsMetrix (Maarssen, The Netherlands) focused on stable labeled fingerprints of two (potassium cyanide trapping assay) or three (glutathione and methoxylamine trapping assays) mass units difference with equal intensity. The equipment consisted of an LTQ-Orbitrap mass spectrometer coupled to an Accela uHPLC from Thermo Scientific. A Hypersil Gold C18 Column (1.9 μm, 2.1×100 mm) from Thermo Scientific with mobile phases of 0.1 % formic acid in water (A) and 0.1 % formic acid in acetonitrile (B) were used. The stepwise linear gradient was 5 % B (0.0–1.0 min), 5–70 % B (1.0–10.0 min), 70–95 % B (10.0–11.0 min), and 95 % B (11.0–13.0 min). The total run time was 15 min using a flow rate of 0.35 ml/min. Capillary temperature was 270 °C with various source, capillary and tube lens voltages in positive ion mode. $MS^2$ was performed on the two most intense peaks that had a mass difference of 3 or 2 Da (both high and low masses of mass tag) with a relative ratio of 80–100 % in the glutathione/methoxylamine and potassium cyanide trapping assays, respectively. $MS^3$ was triggered for neutral loss of *m/z* 129/75/78 in the glutathione trapping assay, *m/z* 27/29 in the potassium cyanide trapping assay and *m/z* 32/35 in the methoxylamine trapping assay. Post-acquisition analysis to make the initial yes/no answer was performed with MsXelerator software to specifically look for isotopic patterns described above. Product ion scan and data interpretation were followed for further confirmation using Xcalibur software (Thermo Scientific, San Jose, CA).

## Microsomal and Plasma Protein Binding

The fraction unbound in human plasma ($f_{up}$) and in HLMs ($f_{umic}$) were determined by equilibrium dialysis using the 96-Well Rapid Equilibrium Dialysis (RED) device from Thermo Scientific (Rockford, IL). Briefly, human plasma (200 μl; pH 7.4) or HLMs (200 μl; 0.6 mg/ml) in PBS (pH 7.4) were spiked with a test article (5 μM final concentration) so that the final solvent concentration was 0.05 % DMSO and 0.95 % acetonitrile. Plasma or microsomes (200 μl) were placed in the donor side of the RED device sample chamber and PBS (350 μl; pH 7.4) was placed on the receiver side; all incubations were performed in triplicate. The plates were sealed with a self-adhesive tape and incubated on an orbital shaker (150 rpm; 37 °C; 4 h). Following incubation, aliquots (30 μl) were taken from the donor and receiver chambers and quenched in acetonitrile (200 μl) containing propranolol (0.1 μM) as internal standard. Blank plasma, HLMs or PBS (30 μl) were added to the appropriate wells to create analytically identical sample matrices to eliminate any matrix effect. Samples were centrifuged (2000×g for 10 min) and aliquots (100 μl) of supernatant were diluted in water (1:1 *v/v*) prior to LC-MS/MS analysis.

Aliquots (10 μl) were analyzed by LC-MS/MS equipment as described earlier for $k_{inact}$ and $K_I$ determination. The mass spectrometer was operated in the positive ion mode and MRM was used to quantify test compound. A Hypersil Gold C18 Column (1.9 μm, 2.1×50 mm) from Thermo Scientific and mobile phases of 0.1 % formic acid in water (A) and 0.1 % formic acid in acetonitrile (B) were used for chromatographic separation using a stepwise linear gradient of 0 % B for (0.0–

0.1 min), 0–98 % B (0.1–1.0 min), 98 % (1.0–2.83 min), and 0 % B (2.84–4.0 min). The total run time was 4 min using a flow rate of 0.4 ml/min.

The compound was quantified using the ratio of test compound peak area to internal standard peak area. Values of $f_{up}$ and $f_{umic}$ were calculated from the ratio of the test compound in buffer (receiver chamber) to the test compound in plasma or microsomes (donor chamber).

### Literature Resources for Clinical PK and DDI Risk

The U.S. National Library of Medicine (http://www.ncbi.nlm.nih.gov/pubmed) and the Drug Approval Packages (http://www.accessdata.fda.gov/scripts/cder/drugsatfda/index.cfm) were the sources of clinical pharmacokinetic and DDI data of drugs confirmed as CYP3A time-dependent inhibitors in these studies. All clinical data were considered, and information on the maximum plasma concentration ($C_{max}$) and AUC from the reported DDI study corresponding to the perpetrator dose were selected and collated along with that at steady state for approved doses (Table I). References associated with clinical data are listed in the Supplementary Material.

### Static Mechanistic Prediction of Drug–Drug Interaction Potential

The potential extent of DDI was predicted according to the method described by Fahmi *et al.* (2008) (26), in which the effects of competitive inhibition and mechanism-based inhibition in both the intestine and liver are incorporated in the model, as illustrated in Eq. 3:

$$\frac{AUC_{po,i}}{AUC_{po}} = \frac{1}{[A \cdot B] \cdot f_{mCYP3A4} + (1 - f_{mCYP3A4})} \cdot \frac{1}{[Y \cdot Z] \cdot (1 - F_G) + F_G} \quad (3)$$

where $AUC_{po,i}$ and $AUC_{po}$ are the areas under the curve of an affected substrate in the presence and absence of an inhibitor, respectively, $F_G$ is the fraction of the substrate that escapes intestinal metabolism, and $f_{mCYP3A4}$ is the fraction of the substrate clearance metabolized by CYP3A4.

The $F_G$ values were taken from Gertz *et al.* (2010) (30) and, whenever possible, were based on estimates obtained from iv and po data ($F_G$ is 0.51 for midazolam and 0.38 for atorvastatin); otherwise, estimates obtained from grapefruit juice studies were used (as in the case of simvastatin, for which $F_G$ is 0.14). Considering intestinal extraction of most of the victim drugs in the dataset (>60%), interaction at the intestine was expected to contribute to the overall DDI magnitude and was therefore considered as physiologically relevant in the mechanistic static model. No data were available for everolimus, so $F_G$ was assumed to be 0.5. The values of $f_{mCYP3A}$ for victim drugs involved in these DDIs were 0.94 for midazolam (19), 0.91 for simvastatin, 0.77 for atorvastatin (31) and 0.93 for everolimus. In the cases of simvastatin and everolimus, $f_{mCYP3A4}$ was estimated from the reported increase in victim drug AUC in the presence of itraconazole (32) and ketoconazole (33), respectively, as 1 - $AUC_{control}/AUC_{+inhibitor}$.

A and Y are the mechanism-based inhibition components in the liver and intestine, respectively; B and Z are the competitive inhibition components in the liver and intestine, respectively. They can be expressed as illustrated in Eqs. 4 and 5:

$$A, Y = \frac{k_{deg}}{k_{deg} + \frac{[I]_u \cdot k_{inact}}{[I]_u + K_I}} \quad (4)$$

$$B, Z = \frac{1}{1 + \frac{[I]_u}{K_I}} \quad (5)$$

where $k_{deg}$ is the rate constant of enzyme degradation. The mean $k_{deg}$ value of 0.03 $h^{-1}$ was used for intestinal CYP3A4 (34,35). In contrast to intestine, there is no consensus on the value of hepatic CYP3A4 $k_{deg}$, and predictions were performed assuming the same $k_{deg}$ in both liver and intestine. In addition, the impact of variability of hepatic $k_{deg}$ (0.0193–0.03 $h^{-1}$, corresponding to a hepatic CYP3A4 turnover half life of 23–36 h; (35)) on the prediction accuracy was also investigated. The inhibitor concentration in the liver was assumed to be either the $C_{max}$ or the average concentration ($C_{av}$) from published clinical studies; the unbound plasma concentration was used for all compounds except gefitinib and sirolimus, for which the unbound blood concentration was reported. The fraction unbound in blood ($f_{ub}$) was estimated from the in-house measured plasma protein binding, and blood-to-plasma ratios were taken from literature resources (Table I). All the inhibition data were corrected for nonspecific microsomal binding based on measurements performed in the current study. The inhibitor concentration in the intestine ($I_G$) was calculated as shown in Eq. 6 assuming no binding of the inhibitor to enterocytic proteins, making $f_{u,gut}$=1 (21):

$$I_G = \frac{Dose \cdot k_a \cdot f_a}{Q_G \cdot Freq} \quad (6)$$

where Dose is total daily dose of an inhibitor given orally, $k_a$ represents the first-order absorption rate constant, $f_a$ represents the fraction of the dose absorbed, $Q_G$ is the intestinal (villous) blood flow (18 l/h; (36)), and Freq is the frequency of daily dose. Under fasted conditions, $f_a$ was assumed to be 0.8, with the exception of erlotinib and nilotinib (0.6 and 0.3, respectively, (37)), and a standard value of 1.8 $h^{-1}$ was used as $k_a$ for all inhibitors (20,26).

**Table I** Clinical Dosing Regimen, Steady State Exposure and *In Vitro* Binding Data for 12 Kinase Inhibitors. Clinical Information and B:P Ratio Collated from Literature Sources as Described in Materials and Methods. The Values of $f_{up}$ and $f_{umic}$ were Measured In-House (Data are Means, $n=3$). References for Clinical Data are Listed in the Supplementary Material

| Kinase inhibitor | Clinical dose/frequency | Steady state $C_{max}$ (ng/ml) | Steady state AUC (ng.h/ml) | B:P ratio | $f_{up}$[a] | $f_{umic}$[a] |
|---|---|---|---|---|---|---|
| Dasatinib | 70 mg BID | 70.5 | 236 | 1.8 | 0.051 | 0.334 |
| Erlotinib | 150 mg QD | 1050 | 18700 | 1.0–1.3 | 0.083 | 0.650 |
| Everolimus | 10 mg QD | 76.7 | 729 | 0.17–0.73 | 0.010 | 0.140 |
| Gefitinib | 250 mg QD | 130 | 2970 | 0.76 | 0.059 | 0.165 |
| Imatinib | 400 mg QD | 2596 | 40100 | 0.42 | 0.118 | 0.433 |
| Lapatinib | 1250 mg QD | 2430 | 36200 | 0.84 | 0.002 | 0.003 |
| Nilotinib | 400 mg BID | 2210 | 16400 | 0.68–0.84 | 0.001 | 0.013 |
| Pazopanib | 800 mg QD | 58000 | 1040000 | 0.59–0.93 | 0.001 | 0.286 |
| Sirolimus | 5 mg QD | 37.4 | 396 | 36.5 | 0.005 | 0.086 |
| Sorafenib | 400 mg BID | 7700 | 64300 | 1.33 | 0.116 | 0.701 |
| Sunitinib | 50 mg QD | 23.2 | 1020 | 1.4 | 0.117 | 0.284 |
| Temsirolimus | 25 mg QW | 443 | 1350 | 3.4 | 0.003 | 0.219 |

*AUC* Area under the curve, *BID* Twice daily, *B:P* Blood-to-plasma partitioning, $C_{max}$ maximum plasma concentration, $f_{up}$ Fraction unbound in human plasma, $f_{umic}$ Fraction unbound in human liver microsomes, *QD* Once daily, *QW* Once weekly

[a] *In vitro* measurement

Prediction accuracy of the hepatic model in isolation or combined with the intestinal interaction was assessed using either $C_{max,u}$ or $C_{av,u}$. When possible, these data were taken from the actual DDI study; alternatively, when only victim drug exposures were reported, data from clinically corresponding doses reported elsewhere were used. In addition, the impact of variability in perpetrator pharmacokinetics was assessed by propagating a 30 % coefficient of variation on AUC and blood binding. The predictive utility of different scenarios was assessed as percent predicted within acceptable limits as proposed recently by Guest *et al.* (2011) (38). The upper and lower prediction limits were more stringent than the commonly used 2-fold in cases in which a minor shift in AUC was expected, approaching the traditional 2-fold limits as the AUC ratio became larger. The limits also accounted for the estimated baseline inter-individual variability in victim drug exposure based on the 20 % variability data observed for midazolam.

## RESULTS

### Assessment of TDI Liability for 5 Major CYP Isoforms

Twenty-six oncology drugs were assessed for TDI. CYP3A was by far the most commonly inhibited isoform with 13 of the drugs exhibiting TDI of CYP3A to some extent (Table II). In all, 12 of the 13 drugs that exhibited TDI were kinase inhibitors. No evidence of TDI was observed for the other 13 drugs evaluated. All of the kinase inhibitors tested were identified as time-dependent inhibitors in this assay, along with the cytotoxic agent docetaxel, although sorafenib was borderline positive on the basis of our criteria (a 15 % AUC shift). CYP3A TDI was assessed using both midazolam and testosterone as probe substrates, and the findings were consistent in both assays, although midazolam tended towards a lower magnitude of inhibition as described by shift in AUC of the $IC_{50}$ curves (shown in Supplementary Material).

Of the 26 drugs evaluated, only three were found to have TDI of isoforms other than CYP3A. This TDI was also confined to the kinase inhibitors, namely gefitinib, nilotinib and sorafenib. Gefitinib inhibited CYP2D6 with a TDI $IC_{50}$ of $2.1\pm0.7$ μM and a shift in AUC of $33\pm8$ %. Nilotinib inhibited CYP2C9 with a TDI $IC_{50}$ of $1.3\pm1.2$ μM and a shift in AUC of $27\pm7$ %. Sorafenib inhibited CYP2C9 and CYP2C19 with TDI $IC_{50}$ values of $1.2\pm1.0$ and $0.9\pm0.6$ μM, respectively, and a shift in AUC of $30\pm17$ and $39\pm19$ %, respectively. However, no further evaluation was performed to investigate this apparent TDI, and confirmation would be required in detailed kinetic assays of the individual isoforms.

### Confirmation and Kinetic Evaluation of CYP3A Time-Dependent Inhibition

Kinetic parameters of CYP3A TDI were determined for 12 kinase inhibitors (Table III). The inhibition observed in the AUC shift assay was confirmed to be both concentration- and time-dependent in this more-detailed assessment of TDI. Close inspection of the kinetic data revealed that the kinase inhibitors fell into three general groups in terms of their inhibition: those whose TDI was simple: dasatinib, erlotinib, imatinib and pazopanib

**Table II** *In Vitro* Time-Dependent CYP3A Inhibition of 26 Oncology Drugs as Assessed by the $IC_{50}$ Shift Assay. Evidence of TDI is Determined by a >15 % Shift in AUC of the $IC_{50}$ Curves Following a 30 min Pre-incubation in the Presence or Absence of NADPH. Data are Means ± SD ($n$=3). Testosterone Was Used as a Probe Unless Otherwise Indicated

| | Drug | Evidence of CYP3A TDI? | % Shift in AUC | TDI $IC_{50}$ ($\mu$M) |
|---|---|---|---|---|
| cytotoxic agent | 5′-Fluorouracil | No | | |
| | Capecitabine | No | | |
| | Cisplatin | No | | |
| | Cyclophosphamide | No | | |
| | Docetaxel[a] | Yes | 45.3 ± 21.2 | 0.1 ± 0.0 |
| | Doxorubicin | No | | |
| | Etoposide | No | | |
| | Irinotecan | No | | |
| | Methotrexate | No | | |
| | Paclitaxel | No | | |
| | Pemetrexed | No | | |
| | Temozolomide | No | | |
| | Topotecan | No | | |
| | Vorinostat | No | | |
| kinase inhibitor | Dasatinib | Yes | 60.2 ± 8.8 | 0.6 ± 0.6 |
| | Erlotinib | Yes | 60.4 ± 12.5 | 1.5 ± 1.8 |
| | Everolimus | Yes | 53.2 ± 11.4 | 0.2 ± 0.1 |
| | Gefitinib | Yes | 33.8 ± 14.0 | 4.8 ± 4.6 |
| | Imatinib | Yes | 58.6 ± 20.6 | 1.0 ± 0.8 |
| | Lapatinib | Yes | 62.1 ± 9.1 | 0.4 ± 0.5 |
| | Nilotinib | Yes | 51.6 ± 13.2 | 0.4 ± 0.4 |
| | Pazopanib | Yes | 59.6 ± 3.2 | 0.3 ± 0.1 |
| | Sirolimus | Yes | 54.8 ± 6.4 | 0.3 ± 0.1 |
| | Sorafenib | borderline | 15.0 ± 9.9 | 1.3 ± 0.1 |
| | Sunitinib | Yes | 33.8 ± 7.4 | 4.9 ± 3.2 |
| | Temsirolimus | Yes | 56.7 ± 5.5 | 0.8 ± 0.8 |

*AUC* Area under the curve, *CYP* Cytochrome P450, *$IC_{50}$* Half maximal inhibitory concentration, *TDI* Time-dependent inhibition

[a] Midazolam was used as a probe

**Table III** Kinetic Parameters of Time-Dependent CYP3A Inhibition for Kinase Inhibitors and Positive Control Troleandomycin. Midazolam was Used as a Probe Substrate Unless Otherwise Stated. Data are Means ± SD ($n$=3)

| Drug | $K_I$ ($\mu$M) | $k_{inact}$ ($min^{-1}$) | $k_{inact}/K_I$ (ml/min/$\mu$mol) |
|---|---|---|---|
| Troleandomycin | 0.62 ± 0.22 | 0.093 ± 0.006 | 160 ± 47 |
| | 0.18 ± 0.06[a] | 0.075 ± 0.002[a] | 424 ± 25[a] |
| Dasatinib | 2.6 ± 1.5 | 0.024 ± 0.002 | 13.6 ± 11.2 |
| Erlotinib | 8.2 ± 1.5 | 0.057 ± 0.004 | 7.1 ± 0.8 |
| Everolimus | 0.9 ± 0.5 | 0.022 ± 0.001 | 34.2 ± 24.6 |
| Gefitinib[a] | 14.1 ± 10.7 | 0.019 ± 0.007 | 2.0 ± 1.1 |
| Imatinib | 4.4 ± 1.5 | 0.028 ± 0.002 | 6.8 ± 2.0 |
| Lapatinib[a] | 4.6 ± 2.8 | 0.029 ± 0.005 | 9.1 ± 7.0 |
| Nilotinib | 1.5 ± 0.9 | 0.033 ± 0.005 | 25.7 ± 9.5 |
| Pazopanib | 2.9 ± 0.9 | 0.021 ± 0.003 | 7.4 ± 1.8 |
| Sirolimus | 0.9 ± 0.2 | 0.027 ± 0.008 | 39.6 ± 18.1 |
| Sorafenib[a] | na | na | na |
| Sunitinib | 31.5 ± 5.4 | 0.020 ± 0.002 | 0.7 ± 0.2 |
| Temsirolimus | 0.6 ± 0.3 | 0.021 ± 0.000 | 42.2 ± 17.6 |

*CYP* Cytochrome P450, *$k_I$* Inhibitor concentration that supports half the maximal rate of inactivation, *$k_{inact}$* Maximal rate of enzyme inactivation, *na* Not appropriate to fit data

[a] Testosterone was used as a probe

(Fig. 2); those for which there was clear evidence of reversible inhibition as well as TDI: everolimus, nilotinib, temsirolimus and sirolimus (Fig. 3), and those for which defining TDI was complicated by apparent activation of metabolism as well as reversible inhibition: gefitinib, lapatinib, sorafenib and sunitinib (Fig. 4).

In the first group the interpretation of kinetic fits was uncomplicated, and maximum inactivation rates were observed at the concentrations tested (Fig. 2). A limiting factor may be solubility for these kinase inhibitors particularly at high concentrations (50 and 100 μM), as no additional inactivation was observed as concentrations increased; this was most apparent for erlotinib for which aqueous solubility is poor (39). By visual inspection, all kinase inhibitors appeared to be in solution up to at least 16 μM. In the second group, a downwards shift in the initial percent remaining control activity at the 0.5 min time point was evidence of a reversible inhibition component, this was particularly clear for sirolimus (Fig. 3). Indeed, for everolimus, nilotinib and sirolimus, reversible inhibition was the predominant mechanism at 50 and 100 μM, and, as such, these data were excluded from the non-linear regression analysis. In the third group, defining TDI was complicated by apparent activation of metabolism as well as reversible inhibition (Fig. 4). These effects were modest for lapatinib and sunitinib, although the reversible inhibition component for lapatinib at 50 and 100 μM was sufficient to overcome the modest activation observed at lower concentrations. Apparent activation was marked for gefitinib and sorafenib, and it was deemed not appropriate to fit kinetic parameters to these compounds despite the fact that inhibition was observed to increase with time.

To evaluate the impact of CYP3A probe selection on the activation of CYP3A metabolism by gefitinib, lapatinib, sorafenib and sunitinib, the kinetic TDI experiments were repeated using testosterone as a probe substrate (Fig. 5). In contrast to the midazolam data, no activation of testosterone metabolism was observed. Thus, it was possible to generate kinetic parameters for gefitinib, and it was now apparent that sorafenib showed no evidence of TDI (although apparent reversible inhibition was observed). Table III shows the kinetic parameters of TDI for the 12 kinase inhibitors, and these values were used in the prediction of clinical DDI risk.

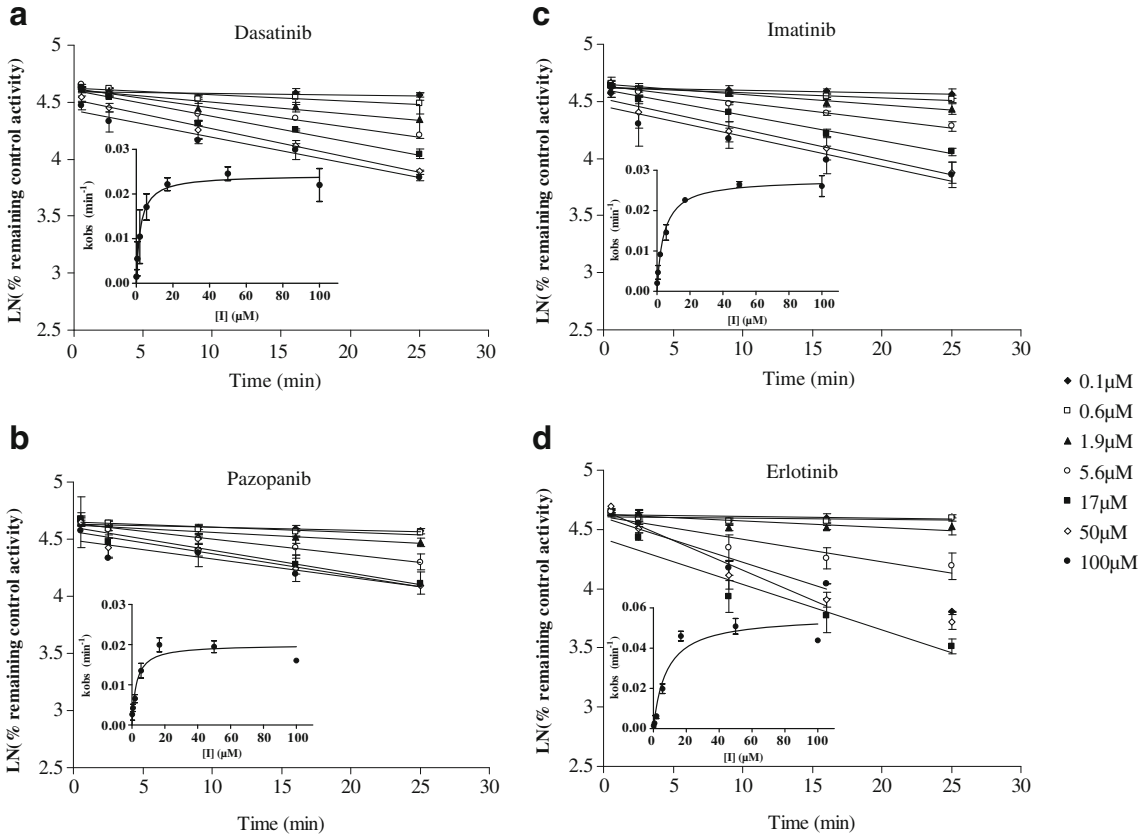


**Fig. 2** Kinetic evaluation of CYP3A time-dependent inhibition for dasatinib (**a**), erlotinib (**b**), imatinib (**c**) and pazopanib (**d**) using midazolam as a probe. Plots of natural log percent remaining control activity verses time show simple time-dependent inhibition with the $k_{obs}$ verses inhibitor concentration fit by non-linear regression inset. Data are means ± SD ($n$=3).

The kinetic parameters generated for erlotinib, imatinib, sunitinib and troleandomycin using midazolam and testosterone as probes were within 2- to 3-fold for both $K_I$ and $k_{inact}$ with no particular trend observed with either probe.

When inspecting the two methodologies used to investigate CYP3A TDI, a good relationship was observed between data generated in the shift assay and the kinetic assay; both the percent shift in AUC and the TDI $IC_{50}$ of the inhibition curves correlated reasonably well with the $k_{inact}/K_I$ ratio (data in Supplementary Material). This is consistent with previous reports of these assays (18,20,40) and demonstrates the utility of a high throughput screening assay for the initial assessment.

## Evidence of Reactive Metabolite Formation for Kinase Inhibitors

Trapping studies were performed using stable labeled glutathione, methoxylamine and potassium cyanide to further investigate the role of bioactivation for these kinase inhibitors, and the results are summarized in Table IV. In order to simplify the data, the ion intensities from the mass spectrometer in full scan mode were binned into four classes, and when several conjugates were present, the conjugate with the highest intensity was reported. These studies showed that all but two of the 12 kinases inhibitors underwent bioactivation to reactive intermediates that were trapped by at least one of the trapping agents. The exceptions were sirolimus and temsirolimus. Gefitinib was positive in all the trapping assays, forming considerable levels of cyanide conjugates. Imatinib was the only other kinase inhibitor to form a cyanide conjugate.

## Prediction of DDI Risk for Kinase Inhibitors Using a Static Mechanistic Model

Eight clinical DDI studies on these kinase inhibitors have been reported, and the magnitude of change in the victim drug AUC was less than 2-fold in all, with the exception of imatinib interaction with simvastatin (3-fold; Table V). To assess the translation of CYP3A TDI *in vitro* to a clinical DDI risk, a static mechanistic model accounting for both TDI and reversible inhibition (where applicable) was applied; use of this model has been well documented in the literature and recommended by the regulatory authorities (www.fda.gov//downloads/Drugs/DevelopmentApprovalProcess/DevelopmentResources/

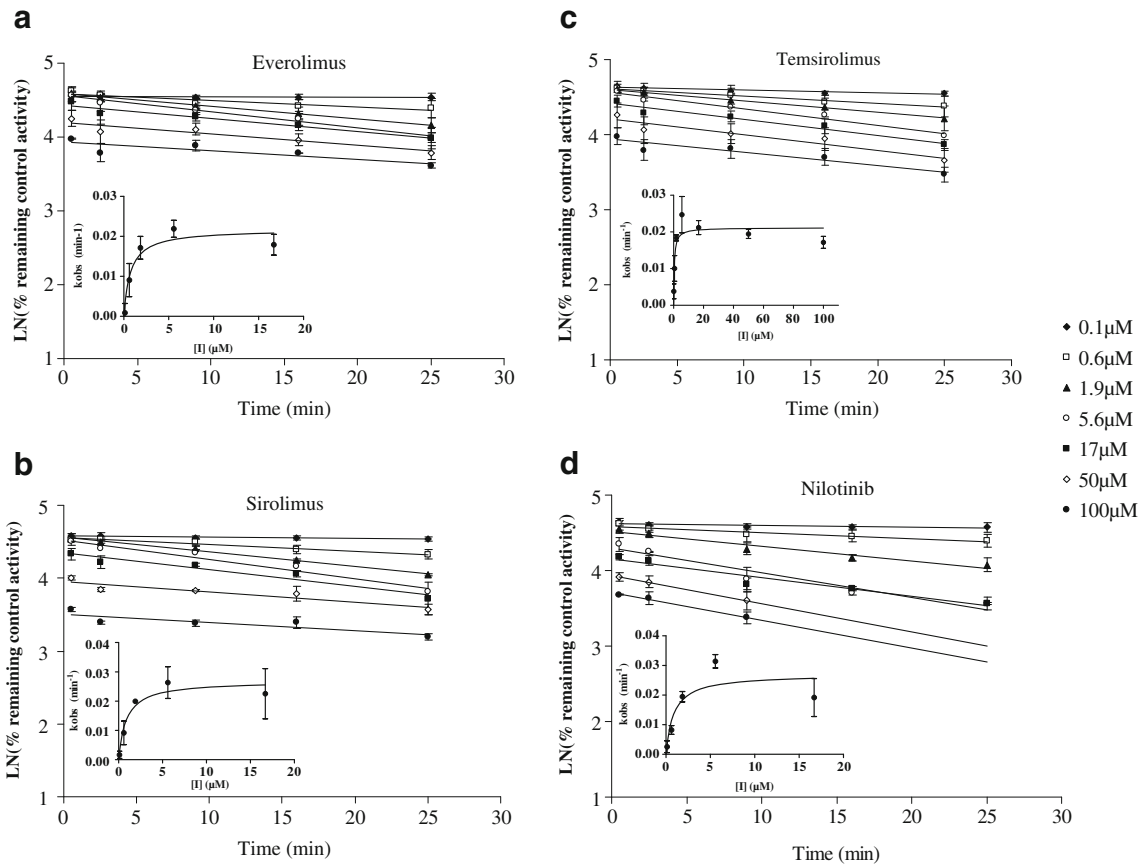


**Fig. 3** Kinetic evaluation of CYP3A time-dependent inhibition for everolimus (**a**), nilotinib (**b**), temsirolimus (**c**) and sirolimus (**d**) using midazolam as a probe. Plots of natural log percent remaining control activity verses time show mixed time-dependent inhibition and reversible inhibition with the $k_{obs}$ verses inhibitor concentration fit by non-linear regression inset. Data are means ± SD ($n$=3).

DrugInteractionsLabeling/UCM269209.pdf) (20,26,41,42). For the purpose of DDI predictions, the *in vitro* TDI data were assumed to reflect CYP3A4 inhibition only. Both $C_{max,u}$ and $C_{av,u}$ were assessed as inhibitor concentration in the model (Table V; Fig. 6), as they are both commonly used in static predictive tools. Use of the model based solely on the hepatic interaction resulted in no false negative predictions and comparable prediction success between $C_{av,u}$ and $C_{max,u}$, with median predicted : observed AUC ratios of 156–204 % (individual values shown in Table V). However, even ignoring the intestinal component led to 38–50 % of DDIs outside the prediction limits; overprediction was more associated with $C_{max,u}$ as the inhibitor concentration choice. Incorporation of intestinal contribution resulted in no false negatives yet DDI overprediction (median predicted : observed AUC ratio of 5.4) (Fig. 6). In the case of imatinib, the magnitude of its DDI with simvastatin was overestimated by more than 10-fold. The analysis was performed assuming the hepatic CYP3A4 recovery half life ($t_{½deg}$) to be either the same (23 h) or longer (36 h) than the intestine; the latter representing the 'worst case' scenario for hepatic $t_{½deg}$ and also encompassing the CYP3A5 degradation half-life (average 36 h, ranging from 15 to 70 h; (43)). Use of a differential and longer hepatic $t_{½deg}$ compared to intestinal $t_{½deg}$ resulted in an increase in the extent of overprediction, as illustrated in Fig. 7; consistent with previous analyses, erlotinib, imatinib, nilotinib and pazopanib were the most pronounced outliers. It was difficult to assess the statistical significance of these overpredictions considering limited availability of the standard deviation data in the clinical studies; nevertheless, the magnitude of clinical DDI is low.

In order to investigate the ability of the static mechanistic model to assess DDI potential of kinase inhibitors, fold-change in the exposure of the standard CYP3A probe midazolam was predicted for four kinase inhibitors, for which no clinical DDI studies were reported. In addition, the same analysis was performed for kinase inhibitors for which an alternative probe to midazolam was used in the actual DDI study. Using the liver-only model and a 1.25-fold change in victim drug AUC as a cut-off indicated that DDIs would be expected with gefitinib, imatinib and lapatinib. Introducing the combined model, weak interactions (<2-fold change in midazolam AUC) were also predicted for sirolimus, sunitinib and temsirolimus with everolimus on the borderline (Fig. 8). Prediction of an erythromycin–midazolam DDI based on in-house generated *in vitro* data was used as a control. Predicted fold-change on the basis of the mechanistic static model and assuming the

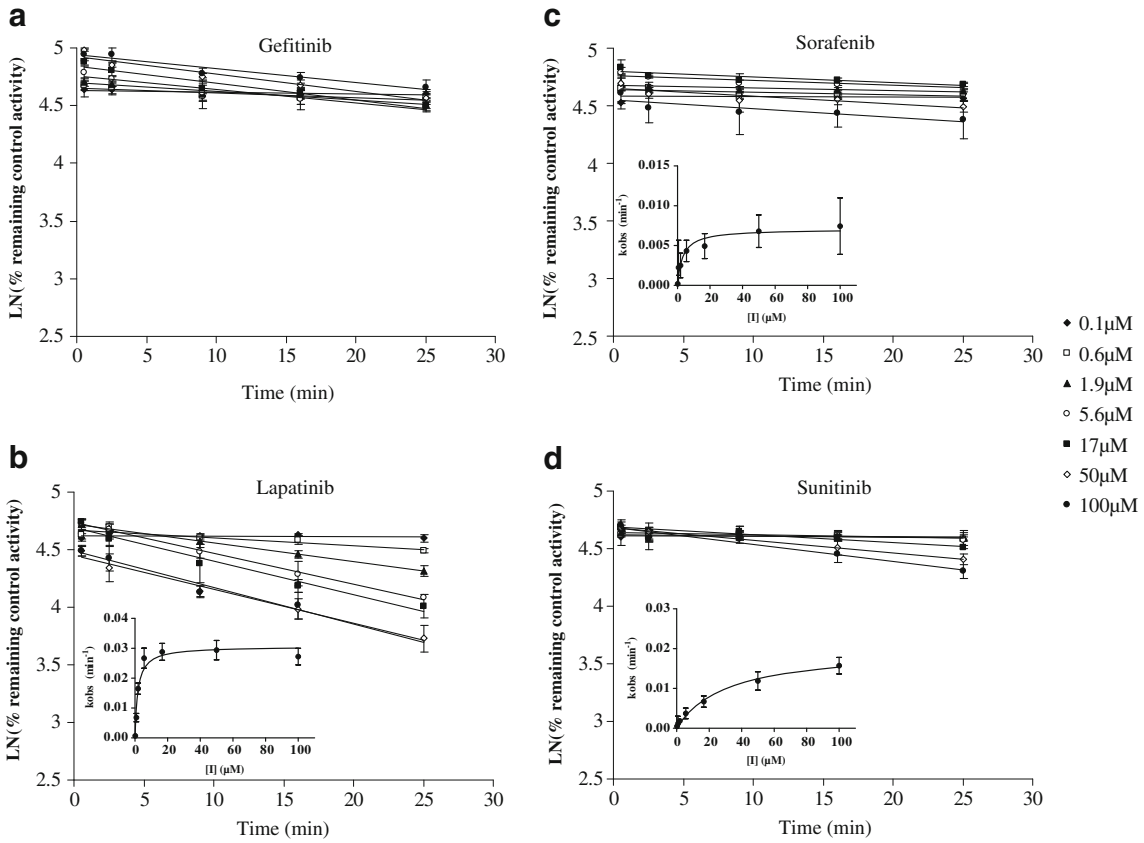


**Fig. 4** Kinetic evaluation of CYP3A time-dependent inhibition for gefitinib (**a**), lapatinib (**b**), sorafenib (**c**) and sunitinib (**d**) using midazolam as a probe. Plots of natural log percent remaining control activity verses time show mixed time-dependent inhibition, reversible inhibition and activation with the $k_{obs}$ verses inhibitor concentration fit by non-linear regression inset where fits were possible. Data are means ± SD ($n$=3).

same CYP3A4 turnover of 23 h in both liver and intestine resulted in a good agreement with the observed erythromycin DDI, with up to 2-fold overprediction depending on the $f_{up}$ used in the model (data not shown).

## DISCUSSION

Protein kinases have emerged as key regulators for all aspects of neoplasia, including proliferation, invasion, angiogenesis and metastasis. Not surprisingly, the development of potent and selective kinase inhibitors for molecularly targeted cancer treatment is considered imperative, and treatment with kinase inhibitors has resulted in significant survival benefit for patients (2). Many oncology therapies are considered narrow therapeutic index drugs and are often used in combination, presenting a risk for potential DDI. This DDI concern is magnified when developing two NME's in combination. Careful consideration of the risk: benefit profile for patients is required and an evaluation of DDI caused by TDI for current marketed drugs is a valuable aid.

In the current study, we evaluated the *in vitro* time-dependent CYP inhibition potential of marketed protein kinase inhibitors alongside other cytotoxic chemotherapeutic agents with a total of 26 marketed oncology drugs in the study. A total of 13 of these drugs were negative for TDI of all CYP isoforms; the other 13 were flagged for potential CYP3A TDI. In the latter subset, three drugs had additional potential for TDI of other CYPs. Of the 12 kinase inhibitors tested, only sorafenib resulted in no TDI of CYP3A. It is perhaps not surprising that the kinase inhibitors featured more prominently with TDI in the group of 26 drugs since they undergo extensive CYP metabolism (Hartmann *et al.*, 2009); docetaxel was the only non-kinase inhibitor tested that exhibited any TDI (CYP3A). An additional point to consider is that many of the cytotoxic agents are actually prodrugs or have high levels of circulating metabolites, so an *in vitro* evaluation of the parent drug alone may not accurately reflect the DDI risks from either a competitive or time-dependent CYP inhibition standpoint (44).

The overall magnitude of TDI for the kinase inhibitors was weak (Table III) in comparison to known clinical time-dependent CYP3A inhibitors such as troleandomycin and mifepristone (in our laboratory, $K_I$=1.3 μM and $k_{inact}$=

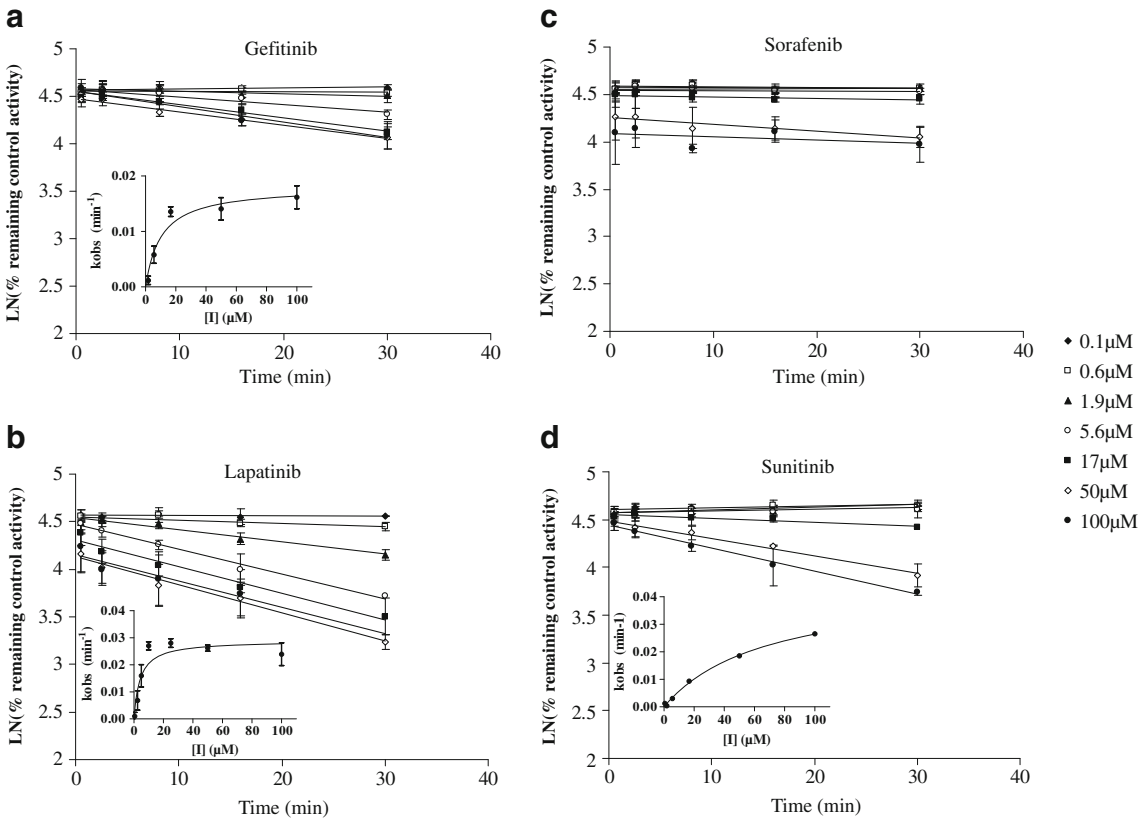


**Fig. 5** Kinetic evaluation of CYP3A time-dependent inhibition for gefitinib (**a**), lapatinib (**b**), sorafenib (**c**) and sunitinib (**d**) using testosterone as a probe. Plots of natural log percent remaining control activity verses time show mixed time-dependent inhibition and reversible inhibition with the $k_{obs}$ verses inhibitor concentration fit by non-linear regression inset where fits were possible. Data are means ± SD ($n$=3).

0.08 $min^{-1}$). Inhibition data presented here are within 2- to 3-fold of published values for dasatinib, erlotinib and lapatinib (14,15,17). It must be noted that no attempt was made to differentiate between inhibition of CYP3A4 or CYP3A5 in the present investigation. Human liver donor demographics for the pooled microsomes used in this study were predominantly Caucasian (86 %); low expression levels relative to CYP3A4 and higher prevalence of less 'functional' CYP3A5*3/*3 are consistent for this population (45,46). Therefore, we have assumed that the TDI parameters determined were reflective of CYP3A4 inhibition. However, this has implications for subsequent clinical DDI risk assessment if the role of CYP3A5 inhibition is not accurately represented or CYP3A4 is over accounted for (45,46).

The correct experimental conditions for *in vitro* TDI assays are critical (18) and kinetic interpretation of data can be complex even under optimal experimental setup (e.g., when protein concentration is as low as possible, the dilution step is maximized and the probe substrate is incubated in excess of $K_m$ for a short period of time). Reversible inhibition may complicate the initial inactivation phase as for the kinase inhibitors grouped in Fig. 3. It is possible that a dilution step in excess of the 20-fold used in this study is necessary. However, in the typical drug discovery screening paradigm, the reversible inhibition component would be known prior to detailed kinetic analysis and so TDI dilution factors could be adjusted accordingly. To further complicate the kinetic analysis, there was evidence that the formation of 1′-hydroxymidazolam was activated by gefitinib and sorafenib and to a lesser extent by lapatinib and sunitinib. The heteroactivation phenomena has previously been reported predominantly, but not exclusively, for CYP3A4 (41,47). Consistent with previous studies, heteroactivation in this study was substrate dependent and observed with midazolam but not testosterone. Heteroactivation of midazolam 1′-hydroxylation has been previously reported *in vitro* in the presence of gefitinib and to a lesser extent erlotinib (48); the authors did not delineate between the effect on CYP3A4 and CYP3A5. By contrast, heteroactivation of midazolam 1′-hydroxylation via CYP3A5 but not CYP3A4 was reported for sorafenib and sunitinib (49). In the current study, no appreciable heteroactivation was detected by erlotinib, but it was observed for sorafenib, sunitinib and lapatinib. The role of CYP3A5 in the apparent activation of midazolam 1′-

**Table IV** Reactive Metabolite Trapping for 12 Kinase Inhibitors in Human Liver Microsomes Using Stable Label Trapping Agents. Relative Intensity is Based on the Ion Intensity from Full Scan Mass Spectrometry in Positive ion Mode. Intensity is Designated as + for 10,000–100,000 cps, ++ for 100,000–500,000 cps, +++ for 500,000–1,000,000 cps and ++++ for >1,000,000 cps. When Several Conjugates Were Present, the Conjugate with the Highest Intensity Was Reported

| Kinase inhibitor | TDI (Yes/No) | Glutathione conjugate intensity (number of conjugates) | Cyanide conjugate intensity (number of conjugates) | Methoxylamine conjugate intensity (number of conjugates) |
|---|---|---|---|---|
| Dasatinib | Yes | ++++ (1) | – | ++++ (2) |
| Erlotinib | Yes | ++ (2) | – | ++++ (2) |
| Everolimus | Yes | – | – | ++ |
| Gefitinib | Yes | +++ (2) | ++++ (8) | +++ (4) |
| Imatinib | Yes | – | ++ (7) | ++ (1) |
| Lapatinib | Yes | +++ (1) | – | ++ (2) |
| Nilotinib | Yes | ++ (1) | – | ++ (2) |
| Pazopanib | Yes | + (1) | – | ++ (2) |
| Sirolimus | Yes | – | – | – |
| Sorafenib | No | ++ (1) | – | – |
| Sunitinib | Yes | + (2) | – | – |
| Temsirolimus | Yes | – | – | – |

*cps* Counts per second, *TDI* Time-dependent inhibition

hydroxylation in these studies is unknown and would need to be explored further considering the differential heteroactivation and inhibition potential reported for CYP3A4 and CYP3A5 (50,51). Comparison of the kinetic parameters generated with either midazolam or testosterone as probe substrates resulted in parameter estimates within 2- to 3-fold for each probe, suggesting that the magnitude of time-dependent CYP inhibition may be independent of the probe used.

Studies were performed to assess bioactivation to reactive intermediates that could be trapped by either glutathione, potassium cyanide or methoxylamine. These agents can trap various types of electrophiles: glutathione traps soft electrophiles such as quinoneimines, nitrenium ions, arene oxides, quinones, imine methides and Michael acceptors (52); cyanide traps iminium ions (28); and methoxylamine traps aldehydes (53). All but two (sirolimus and temsirolimus) of the 12 kinase inhibitors underwent bioactivation to form reactive intermediates that were trapped by at least one of the trapping agents. The trapping data presented here are consistent with previously reported data for dasatinib,

**Table V** Observed and Predicted DDI for Eight of the 12 Kinase Inhibitors for Which Clinical DDI Data was Available. Predictions are Based on Unbound Concentrations Using the Hepatic Model, as Described in the "Materials and Methods" Section, and a CYP3A4 $k_{deg}$ Value of 0.03 $h^{-1}$. References for Clinical Data are Shown in the Supplementary Material

| Kinase inhibitor (perpetrator) | Perpetrator dose/frequency | Perpetrator $C_{max}$ (ng/ml) | Perpetrator AUC (ng.h/ml) | Victim drug | Observed AUC ratio | Predicted AUC ratio[a, b] | Predicted AUC ratio[a, c] |
|---|---|---|---|---|---|---|---|
| Dasatinib | 100 mg SD | 119 | 408 | Simvastatin | 1.23 | 1.1 (6.2) | 1.1 (6.5) |
| Erlotinib | 150 mg QD | nr | nr | Midazolam | 0.9 | | 3.8 (7.1) |
| Everolimus | 2 mg SD | 16.4 | 118 | Atorvastatin | 1.02 | 1.0 (1.8) | 1.1 (2.5) |
| Gefitinib | 250 mg QD | 444 | 3027 | Everolimus | 1.11 | 1.3 (2.5) | 1.3 (2.5) |
| Imatinib | 400 mg QD | nr | nr | Simvastatin | 3.0 | | 5.8 (35.8) |
| Nilotinib | 600 mg, SD | 511 | 14512 | Midazolam | 1.30 | 3.8 (7.4) | 6.0 (11.6) |
| Pazopanib | 800 mg QD | 58000 | 1040000 | Midazolam | 1.35 | 4.3 (8.4) | |
| Sorafenib | 400 mg BID | 4860 | 38130 | Midazolam | 0.85 | 1.0 (1.1) | 1.0 (1.1) |

*AUC* Area under the curve, *BID* Twice daily, $C_{max}$ Maximum plasma concentration, *DDI* Drug–drug interaction, *nr* Not reported in the clinical DDI study, *SD* Single dose, *QD* Once daily

[a] Number in brackets represents the predicted value based on the combined hepatic and intestinal model

[b] Concentrations reported in the clinical DDI study were used in the predictions

[c] Steady state concentrations shown in Table I were used in the predictions

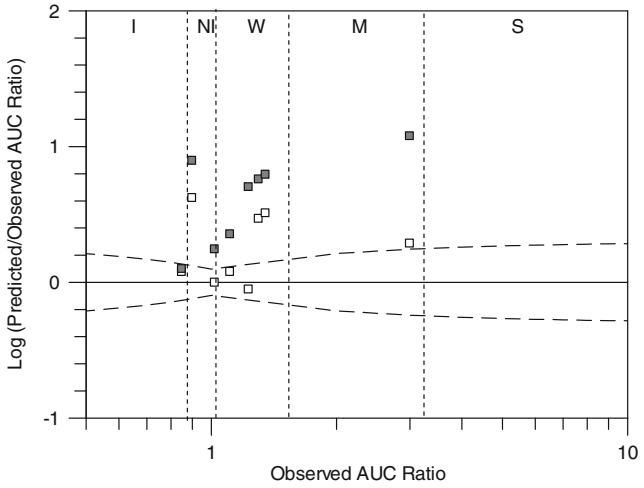


**Fig. 6** Comparison of predicted and observed drug–drug interactions with eight kinase inhibitors based on average unbound concentrations. A) ■ represents hepatic interaction and □ combined hepatic and intestinal model assuming the same CYP3A4 $t_{½deg}$ of 23 h. Dashed lines represent the new predictive measure with inclusion of 20 % variability (Guest *et al.*, 2011). The vertical lines represent the limits between potency classifications, where I, NI, W, M and S represent induction, no interaction, and weak, moderate and strong inhibition interaction, respectively.

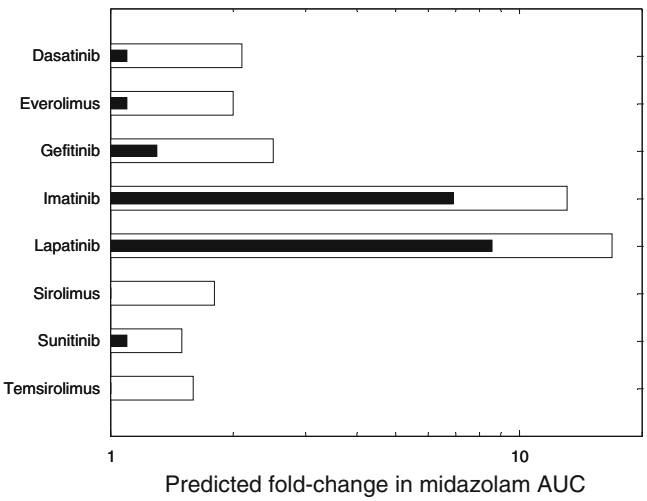


**Fig. 8** Predicted fold-change in midazolam exposure for seven perpetrator drugs with either no reported clinical drug–drug interaction data or with an alternative probe to midazolam. Predictions based on the liver (black bar) and combined model (white bar) and the assumption of the same CYP3A4 $t_{1/2deg}$ of 23 h in the liver and intestine and the use of average unbound concentration.

erlotinib, lapatinib and gefitinib (14–16,54). Interestingly, sorafenib, which was borderline for CYP3A TDI in the $IC_{50}$ shift assay (and flagged for CYP2C9 and CYP2C19 TDI) but negative in the detailed kinetic assays with CYP3A, did form a glutathione conjugate, suggesting that bioactivation does indeed occur. While no direct link exists between these trapping studies and TDI, both pieces of data

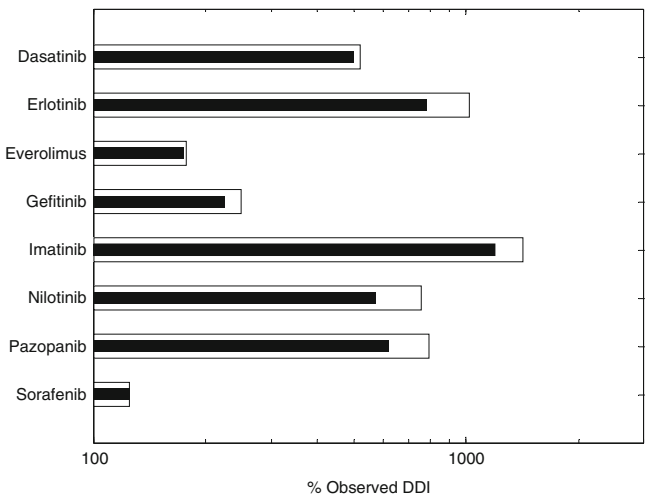


**Fig. 7** Impact of different hepatic CYP3A4 $t_{½deg}$ on the drug–drug interaction (DDI) prediction success expressed as % observed DDI for multiple victim probes. Prediction made using the combined model and the assumption of the same CYP3A4 $t_{½deg}$ of 23 h in the liver and intestine (black bar). White bars represent predictions based on hepatic CYP3A4 $t_{½deg}$ of 36 h; intestinal CYP3A4 $t_{½deg}$ was constant in all the cases. Predictions are based on the use of unbound concentrations as reported in the clinical study.

point towards generation of reactive intermediates capable of covalently modifying protein. However, there is no evidence that the reactive species that is trapped is also responsible for TDI, indeed TDI could be the result of formation of a metabolic intermediate complex as opposed to covalent modification of a heme or CYP apoprotein. Nevertheless, both the TDI and trapping data presented here provide evidence that these kinase inhibitors undergo bioactivation, which has implications in the generation of idiosyncratic adverse drug reactions (55). Relating reactive metabolite formation to clinically significant risk is challenging. One important factor in risk assessment is dose, and it is noteworthy that, with the exception of everolimus, the kinase inhibitor doses (ranging from 100 to 800 mg/day) are on the side of higher risk when considering adverse drug reactions (56). Indeed the link between bioactivation and observed idiosyncratic adverse drug reactions has been drawn in the literature for several kinase inhibitors (14–17).

Static mechanistic $k_{inact}/K_I$ model was used to assess clinical impact of *in vitro* TDI data reported here, using different surrogates for inhibitor concentration (18–20,26,42). Use of the average unbound concentration without considering the intestinal contribution and 1.25-fold as a cut-off for positive DDI, resulted in four true negative predictions (dasatinib, everolimus, gefitinib and sorafenib), one false positive (erlotinib) and three true positive predictions (imatinib, nilotinib and pazopanib) (Table V). Incorporating the intestinal component lead to no false negative predictions, but at the same time resulted in a higher incidence of false positives (Fig. 7). The combined static model correctly assigned 50 % of DDIs: one true negative

(sorafenib) and three true positive predictions (imatinib, nilotinib and pazopanib). The eight DDI studies collated indicate weak *in vivo* DDI for these kinase inhibitors as perpetrators, with the caveat that dasatinib, everolimus and nilotinib DDI data were reported after single dose administration, which would not capture any impact of TDI. Only imatinib results in a victim AUC change of more than 2-fold, and only imatinib, nilotinib and pazopanib have victim AUC ratios greater than 1.25-fold. Considering the high pharmacokinetic variability for oncology drugs (Sparreboom & Verweij (2009) (3) report 25–80 % inter-subject variability in clearance for these kinase inhibitors), defining DDI where AUC change is between 1.25-fold and 2-fold may be statistically challenging. Propagation of 30 % variability in the perpetrator AUC and $C_{av}$ in the current analysis had a marginal impact on the prediction success. In addition, such extensive variability in oral clearance might involve non-linear kinetics, food effects or solubility limited absorption. These factors can certainly contribute to the variability in the inhibitor concentrations available in the liver or intestine and therefore magnitude of DDI and may not be well described by a simple 30 % propagation of variability. Use of a dynamic physiologically-based modeling approach could allow the impact of these factors on DDI to be explored more mechanistically (providing data are available to support it).

An additional area of concern is the fact that all the drugs in the dataset showed extensive plasma protein binding (>90 %) with the exception of imatinib, sorafenib and sunitinib (Table I). Consequently, all the perpetrators had extremely low $f_{up}$; in some instances as low as 0.001 (a level for which accurate determination of the free fraction is difficult). Nilotinib and pazopanib were the most highly bound to plasma proteins, and these two compounds had the greatest degree of DDI overprediction. For most kinase inhibitors, $I_G$ was more than 100-fold higher than $C_{av,u}$, with the exception of imatinib (5-fold difference) and erlotinib, gefitinib and pazopanib (15- to 50-fold). Considering extensive binding of these drugs to plasma proteins (>99 % in a number of cases), binding to enterocytic proteins during absorption cannot be ruled out. However, correction of the $I_G$ estimates for $f_{up}$ had a marginal effect on the extent of overprediction of all kinase inhibitors, with the exception of imatinib. An attempt was made to rationalize the extent of overprediction from the perspective of the victim drugs as well. Despite general confidence in midazolam parameter inputs ($f_{mCYP}$ and in particular $F_G$), it was surprising to see that DDIs with this victim drug were generally overpredicted, in particular the interactions with erlotinib, nilotinib and pazopanib. In contrast, overestimation of atorvastatin and simvastatin DDIs was consistent with previous inhibition and induction DDI database analyses (24), highlighting the need for better understanding of these victim drugs from the mechanistic modeling perspective. For most kinase inhibitors, reversible inhibition does not represent a significant contribution to DDI, and lack of incorporation of this interaction mechanism makes a marginal difference to the prediction success.

The current study critically evaluates the ability of the recommended static mechanistic model to assess DDI potential of oncology drugs; the overall lack of quantitative predictive success with this well-established static model is surprising. The clinical risk of DDI is very modest for kinase inhibitors investigated (as is the *in vitro* TDI in general), and while the model does not result in any false positives, the degree of overestimation is disconcerting and could not be accounted for. Better understanding of the variability associated with the pharmacokinetics of these drugs and elucidation of potential contributing role of CYP3A5 is required. Existing inconsistencies in parameter inputs in TDI static models (e.g., hepatic CYP3A recovery) were supported by the current findings, emphasizing the need for further refinement and consensus on these parameters. These findings do not devalue the utility of this model but suggest additional consideration when inhibition is weak as there is potential for overestimation. Findings of the current study highlight further the necessity for dynamic physiologically-based modeling of DDIs with these kinase inhibitors; work is ongoing to evaluate these models and define whether a more accurate representation of hepatic drug concentrations would improve current predictions.

## CONCLUSION

Many oncology therapies are considered narrow therapeutic index drugs and are often used in combination, presenting a risk for DDI. Careful consideration of the risk:benefit profile for patients is required and an evaluation DDI caused by TDI for current marketed drugs is a valuable aid. Twenty-six oncology drugs were evaluated for TDI, and 13 of the 26 drugs showed no evidence of TDI of any CYP isoform investigated. Overall, 11 of the 12 kinase inhibitors tested were identified as time-dependent inhibitors of CYP3A. The majority of these kinase inhibitors also formed conjugates in assays designed to trap reactive intermediates, thus confirming bioactivation. Using static mechanistic models to predict the clinical DDI potential of these kinase inhibitors as perpetrators resulted in no false negative predictions, but led to overestimation of the DDI magnitude and several false positives, emphasizing the need for more dynamic modeling approaches.

## ACKNOWLEDGMENTS & DISCLOSURES

We thank Dr Cornelis ECA Hop for encouragement to investigate these oncology drugs and members of Genentech DMPK for valuable discussions.

## REFERENCES


1. Riechelmann RP, Del GA. Drug interactions in oncology: how common are they? Ann Oncol. 2009;20(12):1907–12.
2. Giamas G, Man YL, Hirner H, Bischof J, Kramer K, Khan K, *et al.* Kinases as targets in the treatment of solid tumors. Cell Signal. 2010;22(7):984–1002.
3. Sparreboom A, Verweij J. Advances in cancer therapeutics. Clin Pharmacol Ther. 2009;85(2):113–7.
4. Mani S, Ghalib M, Chaudhary I, Goel S. Alterations of chemotherapeutic pharmacokinetic profiles by drug-drug interactions. Expert Opin Drug Metab Toxicol. 2009;5(2):109–30.
5. Traer E, Deininger MW. How much and how long: tyrosine kinase inhibitor therapy in chronic myeloid leukemia. Clin Lymphoma Myeloma Leuk. 2010;10 Suppl 1:S20–6.
6. Banna GL, Collova E, Gebbia V, Lipari H, Giuffrida P, Cavallaro S, *et al.* Anticancer oral therapy: emerging related issues. Cancer Treat Rev. 2010;36(8):595–605.
7. Venkatakrishnan K, Pickard MD, von Moltke LL. A quantitative framework and strategies for management and evaluation of metabolic drug-drug interactions in oncology drug development: new molecular entities as object drugs. Clin Pharmacokinet. 2010;49 (11):703–27.
8. Hartmann JT, Haap M, Kopp H-G, Lipp H-P. Tyrosine kinase inhibitors - a review on pharmacology, metabolism and side effects. Curr Drug Metab. 2009;10(5):470–81.
9. Johnson FM, Agrawal S, Burris H, Rosen L, Dhillon N, Hong D, *et al.* Phase 1 pharmacokinetic and drug-interaction study of dasatinib in patients with advanced solid tumors. Cancer (Hoboken, NJ, U S). 2010;116(6):1582–91.
10. Lathia C, Lettieri J, Cihon F, Gallentine M, Radtke M, Sundaresan P. Lack of effect of ketoconazole-mediated CYP3A inhibition on sorafenib clinical pharmacokinetics. Cancer Chemother Pharmacol. 2006;57(5):685–92.
11. Rakhit A, Pantze MP, Fettner S, Jones HM, Charoin J-E, Riek M, *et al.* The effects of CYP3A4 inhibition on erlotinib pharmacokinetics: computer-based simulation (SimCYP) predicts *in vivo* metabolic inhibition. Eur J Clin Pharmacol. 2008;64(1):31–41.
12. Swaisland HC, Ranson M, Smith RP, Leadbetter J, Laight A, McKillop D, *et al.* Pharmacokinetic drug interactions of gefitinib with rifampicin, itraconazole and metoprolol. Clin Pharmacokinet. 2005;44(10):1067–81.
13. van Erp NP, Gelderblom H, Guchelaar H-J. Clinical pharmacokinetics of tyrosine kinase inhibitors. Cancer Treat Rev. 2009;35 (8):692–706.
14. Li X, He Y, Ruiz CH, Koenig M, Cameron MD. Characterization of dasatinib and its structural analogs as CYP3A4 mechanism-based inactivators and the proposed bioactivation pathways. Drug Metab Dispos. 2009;37(6):1242–50.
15. Li X, Kamenecka TM, Cameron MD. Cytochrome P450-mediated bioactivation of the epidermal growth factor receptor inhibitor erlotinib to a reactive electrophile. Drug Metab Dispos. 2010;38(7):1238–45.
16. Li X, Kamenecka TM, Cameron MD. Bioactivation of the epidermal growth factor receptor inhibitor Gefitinib: implications for pulmonary and hepatic toxicities. Chem Res Toxicol. 2009;22 (10):1736–42.
17. Teng WC, Oh JW, New LS, Wahlin MD, Nelson SD, Ho HK, *et al.* Mechanism-based inactivation of cytochrome P450 3A4 by lapatinib. Mol Pharmacol. 2010;78(4):693–703.
18. Grimm SW, Einolf HJ, Hall SD, He K, Lim H-K, Ling K-HJ, *et al.* The conduct of *in vitro* studies to address time-dependent inhibition of drug-metabolizing enzymes: a perspective of the Pharmaceutical Research and Manufacturers of America. Drug Metab Dispos. 2009;37(7):1355–70.
19. Galetin A, Burt H, Gibbons L, Houston JB. Prediction of time-dependent CYP3A4 drug-drug interactions: impact of enzyme degradation, parallel elimination pathways, and intestinal inhibition. Drug Metab Dispos. 2006;34(1):166–75.
20. Obach RS, Walsky RL, Venkatakrishnan K. Mechanism-based inactivation of human cytochrome P450 enzymes and the prediction of drug-drug interactions. Drug Metab Dispos. 2007;35 (2):246–55.
21. Rowland YK, Jamei M, Yang J, Tucker GT, Rostami-Hodjegan A. Physiologically based mechanistic modelling to predict complex drug-drug interactions involving simultaneous competitive and time-dependent enzyme inhibition by parent compound and its metabolite in both liver and gut-The effect of diltiazem on the time-course of exposure to triazolam. Eur J Pharm Sci. 2010;39 (5):298–309.
22. Wang Y-H. Confidence assessment of the simcyp time-based approach and a static mathematical model in predicting clinical drug-drug interactions for mechanism-based CYP3A inhibitors. Drug Metab Dispos. 2010;38(7):1094–104.
23. Zhang X, Quinney SK, Gorski JC, Jones DR, Hall SD. Semi-physiologically based pharmacokinetic models for the inhibition of midazolam clearance by diltiazem and its major metabolite. Drug Metab Dispos. 2009;37(8):1587–97.
24. Galetin A, Gertz M, Houston JB. Contribution of intestinal cytochrome P450-mediated metabolism to drug-drug inhibition and induction interactions. Drug Metab Pharmacokinet. 2010;25(1):28–47.
25. Mayhew BS, Jones DR, Hall SD. An *in vitro* model for predicting *in vivo* inhibition of cytochrome P450 3A4 by metabolic intermediate complex formation. Drug Metab Dispos. 2000;28(9):1031–7.
26. Fahmi OA, Maurer TS, Kish M, Cardenas E, Boldt S, Nettleton D. A combined model for predicting CYP3A4 clinical net drug-drug interaction based on CYP3A4 inhibition, inactivation, and induction determined *in vitro*. Drug Metab Dispos. 2008;36 (8):1698–708.
27. Halladay JS, Delarosa EM, Tran D, Wang L, Wong S, Khojasteh SC. High-throughput, 384-well, LC-MS/MS CYP inhibition assay using automation, cassette-analysis technique and streamlined data analysis. Drug Metab Lett. 2011;5(3):220–30.
28. Argoti D, Liang L, Conteh A, Chen L, Bershas D, Yu C-P, *et al.* Cyanide trapping of iminium ion reactive intermediates followed by detection and structure identification using liquid chromatography-tandem mass spectrometry (LC-MS/MS). Chem Res Toxicol. 2005;18(10):1537–44.
29. Yan Z, Maher N, Torres R, Caldwell GW, Huebert N. Rapid detection and characterization of minor reactive metabolites using stable-isotope trapping in combination with tandem mass spectrometry. Rapid Commun Mass Spectrom. 2005;19(22):3322–30.
30. Gertz M, Harrison A, Houston JB, Galetin A. Prediction of human intestinal first-pass metabolism of 25 CYP3A substrates from *in vitro* clearance and permeability data. Drug Metab Dispos. 2010;38 (7):1147–58.
31. Houston JB, Galetin A. Methods for predicting *in vivo* pharmacokinetics using data from *in vitro* assays. Curr Drug Metab. 2008;9 (9):940–51.
32. Neuvonen PJ, Kantola T, Kivisto KT. Simvastatin but not pravastatin is very susceptible to interaction with the CYP3A4 inhibitor itraconazole. Clin Pharmacol Ther. 1998;63(3):332–41.
33. Kovarik JM, Beyer D, Bizot MN, Jiang Q, Shenouda M, Schmouder RL. Blood concentrations of everolimus are markedly increased by ketoconazole. J Clin Pharmacol. 2005;45(5):514–8.
34. Gertz M, Harrison A, Houston JB, Galetin A. Prediction of human intestinal first-pass metabolism of 25 CYP3A substrates from *in vitro* clearance and permeability data. Drug Metab Dispos. 2010;38 (7):1147–58.
35. Yang J, Liao M, Shou M, Jamei M, Yeo KR, Tucker GT, *et al.* Cytochrome P450 turnover: regulation of synthesis and

degradation, methods for determining rates, and implications for the prediction of drug interactions. Curr Drug Metab. 2008;9 (5):384–93.
36. Yang J, Jamei M, Yeo KR, Tucker GT, Rostami-Hodjegan A. Prediction of intestinal first-pass drug metabolism. Curr Drug Metab. 2007;8(7):676–84.
37. Duckett DR, Cameron MD. Metabolism considerations for kinase inhibitors in cancer treatment. Expert Opin Drug Metab Toxicol. 2010;6(10):1175–93.
38. Guest EJ, Aarons L, Houston JB, Rostami-Hodjegan A, Galetin A. Critique of the two-fold measure of prediction success for ratios: application for the assessment of drug-drug interactions. Drug Metab Dispos. 2011;39(2):170–3.
39. Ozaki S, Minamisono T, Yamashita T, Kato T, Kushida I. Supersaturation-nucleation behavior of poorly soluble drugs and its impact on the oral absorption of drugs in thermodynamically high-energy forms. J Pharm Sci. 2011;No pp. yet given.
40. Burt HJ, Galetin A, Houston JB. IC50-based approaches as an alternative method for assessment of time-dependent inhibition of CYP3A4. Xenobiotica. 2010;40(5):331–43.
41. Galetin A, Clarke SE, Houston JB. Multisite kinetic analysis of interactions between prototypical CYP3A4 subgroup substrates: midazolam, testosterone, and nifedipine. Drug Metab Dispos. 2003;31(9):1108–16.
42. Wang YH, Jones DR, Hall SD. Prediction of cytochrome P450 3A inhibition by verapamil enantiomers and their metabolites. Drug Metab Dispos. 2004;32(2):259–66.
43. Rendic S. Summary of information on human CYP enzymes: Human P450 metabolism data. Drug Metab Rev. 2002;34(1 & 2):83–448.
44. Yeung CK, Fujioka Y, Hachad H, Levy RH, Isoherranen N. Are circulating metabolites important in drug-drug Interactions?: quantitative analysis of risk prediction and inhibitory potency. Clin Pharmacol Ther (N Y, NY, U S). 2010;89(1):105–13.
45. Lin YS, Dowling ALS, Quigley SD, Farin FM, Zhang J, Lamba J, *et al.* Co-regulation of CYP3a4 and CYP3a5 and contribution to hepatic and intestinal midazolam metabolism. Mol Pharmacol. 2002;62(1):162–72.
46. Xie H-G, Wood AJJ, Kim RB, Stein CM, Wilkinson GR. Genetic variability in CYP3A5 and its possible consequences. Pharmacogenomics. 2004;5(3):243–72.
47. Hutzler JM, Tracy TS. Atypical kinetic profiles in drug metabolism reactions. Drug Metab Dispos. 2002;30(4):355–62.
48. Li J, Zhao M, He P, Hidalgo M, Baker SD. Differential metabolism of gefitinib and erlotinib by human cytochrome P450 enzymes. Clin Cancer Res. 2007;13(12):3731–7.
49. Sugiyama M, Fujita K-I, Murayama N, Akiyama Y, Yamazaki H, Sasaki Y. Sorafenib and sunitinib, two anticancer drugs, inhibit CYP3A4-mediated and activate CY3A5-mediated midazolam 1′-hydroxylation. Drug Metab Dispos. 2011;39(5):757–62.
50. Henshall J, Galetin A, Harrison A, Houston JB. Comparative analysis of CYP3A heteroactivation by steroid hormones and flavonoids in different *in vitro* systems and potential *in vivo* implications. Drug Metab Dispos. 2008;36(7):1332–40.
51. McConn II DJ, Lin YS, Allen K, Kunze KL, Thummel KE. Differences in the inhibition of cytochromes P450 3A4 and 3A5 by metabolite-inhibitor complex-forming drugs. Drug Metab Dispos. 2004;32(10):1083–91.
52. Evans DC, Watt AP, Nicoll-Griffith DA, Baillie TA. Drug-protein adducts: an industry perspective on minimizing the potential for drug bioactivation in drug discovery and development. [Erratum to document cited in CA140:138559]. Chem Res Toxicol. 2005;18(11):1777.
53. Goldszer F, Tindell GL, Walle UK, Walle T. Chemical trapping of labile aldehyde intermediates in the metabolism of propranolol and oxprenolol. Res Commun Chem Pathol Pharmacol. 1981;34 (2):193–205.
54. Takakusa H, Wahlin MD, Zhao C, Hanson KL, New LS, Chan ECY, *et al.* Metabolic intermediate complex formation of human cytochrome P450 3A4 by lapatinib. Drug Metab Dispos. 2011;39 (6):1022–30.
55. Riley RJ, Grime K, Weaver R. Time-dependent CYP inhibition. Expert Opin Drug Metab Toxicol. 2007;3(1):51–66.
56. Park BK, Boobis A, Clarke S, Goldring CEP, Jones D, Kenna JG, *et al.* Managing the challenge of chemically reactive metabolites in drug development. Nat Rev Drug Discovery. 2011;10(4):292–306.